



HAL
open science

Self-organization and tunable characteristic lengths of two-dimensional hexagonal superlattices of nanowires directly grown on substrates

Deliang Yi, Laurent Peres, Alexandre Pierrot, Simon Cayez, Robin Cours, Bénédicte Warot-Fonrose, Cécile Marcelot, Pierre Roblin, Katerina Soulantica, Thomas Blon

► **To cite this version:**

Deliang Yi, Laurent Peres, Alexandre Pierrot, Simon Cayez, Robin Cours, et al.. Self-organization and tunable characteristic lengths of two-dimensional hexagonal superlattices of nanowires directly grown on substrates. *Nano Research*, 2022, 10.1007/s12274-022-4804-6 . hal-03740858

HAL Id: hal-03740858

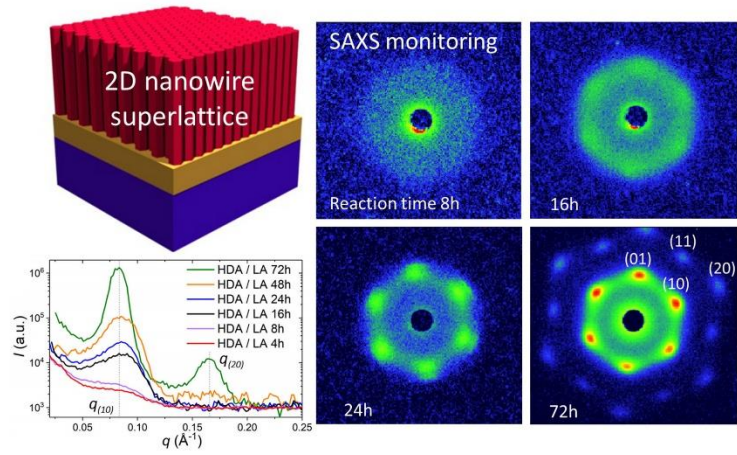
<https://hal.science/hal-03740858>

Submitted on 2 Aug 2022

HAL is a multi-disciplinary open access archive for the deposit and dissemination of scientific research documents, whether they are published or not. The documents may come from teaching and research institutions in France or abroad, or from public or private research centers.

L'archive ouverte pluridisciplinaire **HAL**, est destinée au dépôt et à la diffusion de documents scientifiques de niveau recherche, publiés ou non, émanant des établissements d'enseignement et de recherche français ou étrangers, des laboratoires publics ou privés.

graphical Table of Contents



Using a combined analysis of small angle X-ray scattering, transmission and scanning electron microscopies, we demonstrate the direct growth on surfaces of metallic nanowires which self-organize into highly ordered hexagonal superlattices with tunable characteristics lengths depending of the used stabilizing surfactants.

**Self-organization and tunable characteristic lengths of two-dimensional hexagonal
superlattices of nanowires directly grown on substrates**

D. Yi¹, L. Peres¹, A. Pierrot¹, S. Cayez¹, R. Cours², B. Warot-Fonrose², C. Marcelot², P.
Roblin³, K. Soulantica¹, T. Blon^{1,*}

¹ Université de Toulouse, Laboratoire de Physique et Chimie des Nano-Objets, UMR 5215

INSA, CNRS, UPS, 135 Avenue de Rangueil, F-31077 Toulouse, cedex 4, France

² CEMES, Université de Toulouse, CNRS, 29 Rue Jeanne Marvig, BP 94347, F-31055

Toulouse, France

³ Laboratoire de Génie Chimique, Université de Toulouse, CNRS, INP, UPS Toulouse,

France

* corresponding author: thomas.blon@insa-toulouse.fr

Abstract

The organization of nano-objects on macroscopic surfaces is a key challenge for the technological improvement and implementation of nanotechnologies. For achieving operational functions, it is required to assemble nano-objects as controllable building blocks in highly ordered superstructures. Here we demonstrate the growth and self-organization of metallic nanowires on surfaces into hexagonal superlattices with tunable characteristics lengths depending of the used stabilizing surfactants. Starting from a reacting mixture containing a Pt(111) substrate, a Co organo-metallic precursor, an amine and an acid dissolved in a solvent, we quantify the structural evolution of superlattices of vertical single-crystalline Co nanowires on Pt using a combined analysis of small angle neutron scattering, transmission and scanning electron microscopies. It is shown the concerted steps of growth and self-organization of the nanowires into a spontaneous 2D hexagonal lattice on Pt, at intervals starting from a few hours of reaction to a highly ordered superlattice at longer times. Furthermore, it is shown that apart from long-chain acid and long chain aliphatic amine pairs used as stabilizers, the combination of a long chain aliphatic and a short aromatic ligand in the synthesis can be also employed for the nanowire superlattices development. Interestingly the possibility to employ different pairs allows quantitative modulation of the nanowire arrays, such as the interwire distance and the packing fraction.

Keywords : metallic nanowire array, self-assembly, self-organized growth, Co nanowire, anisotropic growth, solution epitaxial growth

1. INTRODUCTION

The long-range organization of nano-objects on surfaces is an objective pursued in numerous topics of nanotechnology, for instance nanoelectronics, nanoparticle-based sensors, magnetic data storage, metamaterials, etc. Nanostructuring and nanopatterning techniques based on lithography and etching processes allow reducing pattern dimensions while keeping uniformity, with the drawbacks of being time consuming, expensive and possibly detrimental for the etched materials. Self-assembly of colloidal nanocrystals by solvent evaporation is particularly interesting for obtaining periodically ordered, well crystallized and monodispersed nano-objects [1,2,3], but interplays between physical and chemical mechanisms driving self-assembly complexify the processes and limit the long-range order [4]. Direct growth of self-organized nanocrystals on surfaces is a very attractive alternative [5]. As a pure bottom-up approach, it should offer relatively high fabrication rate with large processed areas, while keeping small tolerances in terms of size and shape [6-8]. A promising strategy toward a direct integration of nanocrystals on surfaces exploits wet-chemistry nanoparticle synthesis of inorganic, hybrid and/or multifunctional complex nano-objects, in the presence of planar seeds. Elongated nano-objects are particularly well suited for their direct growth on surfaces due to their intrinsic unidirectional growth [9-12]. Moreover, the collective properties depend not only on the intrinsic characteristics of the individual building blocks such as size and shape, but also on the spatial arrangement between them [8,13]. It is thus crucial to define global bottom-up processes allowing the control of the nanoparticle separation distance. As solution grown particles consist in an inorganic core coated with an organic ligand corona preventing coalescence, one way to achieve nanoparticle superlattice modulations is to act on the nature of ligands introduced in the reaction. This step is not trivial because, apart from preventing coalescence, ligands also determine the features of the resulting nano-objects. Indeed, ligands can form prenucleation species that, depending on the ligand nature, are more or less prone to

reduction. In this way they affect the kinetics of the nanoparticle nucleation and growth. In addition, due to their different affinity for different crystallographic facets of the nanocrystals, they can favor the stabilization of certain types of facets which will *in fine* grow at the expense of some others. These effects define both nanocrystal size and shape. In this context, by adapting the solution synthesis of Co nanorods [14-15], we previously showed the epitaxial growth of Co nanowires (NWs) on crystalline thin films [16] and bulk metal foams [17]. This approach has been extended to liquid phase syntheses of Fe [18] and Pt nanoparticles, to directly grow Fe and Pt nanocubes and prisms on substrates [19,20]. Due to the epitaxial growth, the relationship between the crystalline symmetries of the nanocrystals and of the surface of the films allows driving the orientation of the supported nanostructures, while the solution composition defines the shape [6,7]. However, acting on the nature of the introduced ligands to modulate the nanoparticle superstructure while maintaining a defined shape represents a key challenge. Here, as a model system, we focus on the solution epitaxial growth of Co nanowire (NWs) arrays on Pt films using different aliphatic and aromatic ligands to examine the nanowire growth, the superlattice formation and possible control of the packing fraction. Indeed, tuning the interwire distance and density in arrays of magnetic nanocrystals, such as Co nanowires, is particularly interesting for future magnetic data storage where next generation of hard disk drives are thought to be based on bit patterned media where each magnetic element should be located at precise location on the disk [16,21,22]. Therefore, structural evolution of the NW assembly during growth was monitored through a combined analysis of small angle neutron scattering (SAXS) [23], scanning electron microscopy (SEM) and transmission electron microscopy (TEM). We prove the ability of pairs of aliphatic/aromatic ligands to (i) induce the direct growth of 2D hexagonal arrays of nanowires on substrates, and (ii) to modulate the characteristic lengths of the superlattices such as the NW diameter, interwire distance and packing fraction.

2. RESULTS and DISCUSSION

Briefly, the synthesis consists in the introduction of a Pt(111) epitaxial film on a single crystalline $\text{Al}_2\text{O}_3(0001)$ substrate into a toluene solution containing the Co precursor $[\text{Co}\{\text{N}(\text{SiMe}_3)_2\}_2(\text{thf})]$, a carboxylic acid and an amine. We had previously shown that the matching between the 6-fold symmetry surface of Pt(111) films and *hcp* Co(0001) NW growing planes allows the vertical growth of the Co NWs: the nanowire long axis corresponding to Co[0001] is parallel to Pt[111] [20]. The amines used here are hexadecylamine (HDA) or benzylamine (BA) and the carboxylic acids were lauric acid (LA) or phenylacetic acid (PAA). This choice was made in order to determine the way the different nature of the amine or the acid can affect the superlattice characteristics. It has to be noted that the electronic and/or steric properties of the ligands may affect the reaction outcome by acting on different stages of the nanoparticle growth (stability of prenucleation species, kinetics of nucleation and growth, stabilization of the exposed facets). We have thus compared pairs of (i) two long-chain ligands (HDA/LA), (ii) a short-chain amine comprising a phenyl ring with a long-chain acid (BA/LA), (iii) a long-chain amine with a short chain acid comprising a phenyl ring (HDA/PAA), and finally (iv) two short-chain ligands comprising a phenyl ring (BA/PAA). The combination of a short-chain aliphatic amine and a short-chain aliphatic acid does not produce nanorods of homogeneous dimensions as we have verified in the seedless version of the reaction, *i.e.* in the absence of support. Since what happens in the seedless version is closely related to what happens in the presence of a support, this combination was excluded from our study. Unless otherwise stated, the solution was heated at 110°C under 3 bar of H_2 . After different reaction times, the Pt films were removed from the reactor, dried and observed by SEM, then by SAXS in transmission mode (normal to the substrate) and finally by cross-sectional TEM.

Figure 1 displays (i) SEM, (ii) cross-sectional TEM micrographs, and (iii) 2D SAXS patterns of the samples obtained after different reaction times from solutions containing the Co precursor, HDA and LA. For sufficiently long reaction times, the SEM micrographs of the sample surface reveal dense arrays of NWs, homogeneously covering the entire substrate area, whereas for reaction times as low as 4h, SEM does not clearly reveal their presence. Both SEM and TEM show bundles of nanowires formed during solvent evaporation. The TEM cross-section images confirm the vertical growth of Co NWs on Pt(111) and allow measuring their individual dimensions: the nanowire length varies linearly between 35 nm (4h) and 700 nm (72h) as a function of the reaction time, while the NW diameter D is constant with respect to the reaction time, presenting an averaged value $\langle D_{HDA/LA} \rangle = 6.25$ nm and standard deviation $\sigma = 0.59$ nm on the 4-72h time range (Fig. S1, Supplementary Information).

The corresponding SAXS patterns recorded from samples obtained at different reaction times are displayed on Figure 1(iii). While at short reaction times (4 and 8 hours) SAXS does not reveal any organized pattern, starting from 16h reaction (Fig. 1(iii) (d)) a 6-fold symmetry pattern was recorded in reciprocal space corresponding to a lattice of 2D hexagonally arranged NWs. For the longest reaction time, 72h, the long-range order is attested by the presence of reflections referred as (hk) Bragg indices corresponding to the 2D hexagonal lattice of Co NWs (Fig. S2, Supplementary Information): (10), the associated second order (20), and (11).

Interestingly, this method of fabrication of self-organized NW arrays directly grown on the solid support is closely related to the synthesis of freestanding mesocrystals of cobalt nanorods in solution [24]. Despite the different reaction conditions (temperature, reactant concentration, absence of support), the freestanding nanorod superlattices obtained in the absence of solid support share common characteristics with the NW lattices grown here on Pt(111). Indeed, in both cases the individual nano-objects growth and their organization takes place

simultaneously. In addition, growth takes place along their long axis, while the diameter is stable throughout the growth process (Fig. S1, Supplementary Information). The long-chain amine and acid play a major role in the nanorod growth mechanism and concerted growth–organization process. It has been also shown that the variation of the carbon chain length of the acid length induces modifications of the nanorod dimensions, albeit, clear tendencies associating the chain length to the nanorod dimensions have not been established [25]. In this context, a modification of the acid and/or the amine should impact the NW growth and should allow tuning of the NW diameter and/or the ligand shell thickness, and, through this, the distance between NWs on the solid support.

In a first step, we substituted LA by PAA while HDA was conserved. We successfully obtained arrays of Co NWs as displayed in SEM, TEM and SAXS images presented in Figure 2 (columns *i*, *ii*, and *iii* respectively). The Pt surface is covered with vertical nanowires and 6-fold symmetry SAXS patterns were recorded confirming the ability of the HDA/PAA amine/acid combination to induce the growth and self-organization processes on Pt(111): the long-range order of the 2D hexagonal lattice of NWs is certified by (10), (20) and (11) reflections. The TEM analysis indicates that the nanowire diameter is constant over the reaction time range with $\langle D_{HDA/PAA} \rangle = 6.43$ nm and $\sigma = 0.80$ nm (Fig. S3, Supplementary Information).

Figure 3 displays the Co NWs arrays obtained after synthesis using BA which substituted HDA while conserving LA. In this case, the reaction temperature was slightly increased to 130°C in comparison to other amine/acid pairs because synthesis at 110°C did not lead to the Co growth on Pt. Note that for Co/HDA/LA synthesis, increasing the reaction temperature at 150°C [16] resulted in the same NW diameter and interwire distance as reported here at 110°C suggesting that at this temperature range the NW dimensions were not affected. Figure 3 shows that the synthesis performed with the BA/LA amine/acid pair also led to vertical Co NWs on Pt(111)

organized into a single crystalline hexagonal lattice. Here also the NW diameter keeps unchanged for different reaction times, with however a smaller value than for precedent cases, that is $\langle D_{BA/LA} \rangle = 6.06$ nm and $\sigma = 0.45$ nm (Fig. S4, Supplementary Information).

As the three HDA/LA, BA/LA and HDA/PAA amine/acid pairs led to hexagonal Co NWs arrays, a final question concerns the ability of the combination of BA and PAA pair to achieve the growth/self-organization process. Figure 4 displays the results of the synthesis based on the Co/BA/PAA ratio 1/2/2, $[Co] = 15$ mM, at 110 °C in toluene. The TEM cross-sectional analysis revealed large columns of Co (9-10 nm) grown perpendicularly to the Pt(111) surfaces, which contrasts with the nanowires described above. Particularly, the SAXS pattern and the $I(q)$ analysis do not evidence any structural order nor characteristic length.

The quantitative comparison of the HDA/LA, HDA/PAA and BA/LA amine/acid pairs that lead to NWs superlattices are presented in Figure 5. Figures 5(a), (b) and (c) display the radial intensity profiles $I(q)$ performed along the (10) and (20) Bragg reflections of the SAXS patterns for HDA/LA, HDA/PAA and BA/LA pairs, respectively. For HDA/LA, whereas the hexagonal spontaneous organization is qualitatively evidenced from 16h of reaction, the intensity profiles $I(q)$ obtained for reaction times as short as 4h and 8h exhibit the (10) feature, which means that the hexagonal packing of the NWs initiates very early during the synthesis with a defined interwire distance. The center-to-center distance d between nearest neighboring NWs is calculated using $q_{(10)} = \frac{2\pi}{d_{(10)}} = \frac{4\pi}{\sqrt{3}d}$, where $q_{(10)}$ is the reciprocal vector length corresponding to the $d_{(10)}$ -spacing of (10) planes of the 2D Co NW hexagonal lattice (Fig. S2, Supplementary Information). Figure 5(d) plots the center-to-center interwire distances d obtained for all amine/acid pairs as a function of reaction time. This confirms that the interwire distance d is fixed early during the reaction (4h for HDA/LA) and, as the reaction continues, it keeps

practically constant, while the NW length increases linearly (Fig. 5(e)). The interwire distance, or else the interstitial gap between the NWs due to the organic ligand shell, were quantitatively deduced from the difference between the mean center-to-center interwire distance d and the NW diameter D measured on TEM micrographs of the three acid amine pairs (see Figs. S1-S3 and S4, Supplementary Information), for each reaction time. The resulting ligand shell thicknesses are plotted in Figure 5(f) as a function of the reaction time for the different amine/acid pairs. Table 1 compares the NW growth rate (estimated from linear fits of the NW lengths vs reaction time Fig. 5(e)), mean interwire distance d (from Fig. 5(d)), NW diameter D , ligand shell thickness (from Fig. 5(f)) and the corresponding hexagonal packing fraction $P = (\pi/2\sqrt{3}) \cdot (D/d)^2$ of the Co NWs arrays. The interwire distance and packing are not significantly affected by substituting lauric acid by phenylacetic acid. Indeed, the measured values of the NW diameter and the shell thickness are marginally different and within experimental error. On the other hand, the use of benzylamine instead of hexadecylamine succeeded in tuning the interwire distance and therefore packing fraction.

Table 1: comparative properties of the Co NWs arrays obtained with different amine/acid pairs.

Amine / Acid	NW growth rate (nm/h.)	Mean NW diameter D (nm)	Mean center-to-center interwire distance d (nm)	Mean ligand shell thickness $d - D$ (nm)	Packing fraction P	L/R
HDA / LA	8.8 ± 1.3	6.25 ± 0.59	8.44 ± 0.14	2.13 ± 0.51	0.50 ± 0.09	0.65
HDA / PAA	5.8 ± 2.9	6.43 ± 0.80	9.00 ± 0.20	2.38 ± 0.49	0.46 ± 0.12	0.63
BA / LA	4.8 ± 1.7	6.06 ± 0.45	9.97 ± 0.70	3.83 ± 0.45	0.34 ± 0.07	0.51

The structural characteristics of the superlattices are not straightforward to rationalize based on the dimensions of the ligands employed. The length of the fully extended carbon long chain ligands can be approximated by $L = (n + 1)0.12$ nm, where n is the carbon number of

the ligand [26]. Thus, the lengths of HDA and LA are evaluated to be about 2.04 nm and 1.56 nm respectively. Ligand-ligand, ligand-solvent interactions as well as the effective softness parameter (L/R ratio where R is the nanoparticle radius, calculated in Table 1 considering the longest ligand involved) determine the effective nanocrystal radius in spherical nanocrystal self-assemblies prepared by solvent evaporation of solvated nanocrystals and by variation of the ligands [27-28]. Here rationalization of the superlattices structure based on the L/R ratio would be very speculative since the formation of the NW superlattices during NW growth are also governed by intricate chemical reactions that take place during the nucleation and growth steps. Indeed, it has been shown recently that cobalt nanorods obtained from HDA/LA mixtures under very similar reaction conditions are stabilized by a mixture of laurate and hexadecyl laurylamide, resulting from a condensation between the ligands under the reaction conditions [29]. As often reported in dried superlattices of nanocrystals [26-28], the mean interstitial distance (here 2.13 nm in the HDA/LA system) is significantly shorter than what would be expected from a simple bilayer of either LA or hexadecyl laurylamide in the absence of intercalation between ligands of vicinal NWs. We thus assume that intercalation takes place independently of the nature of the ligand layer. Assuming that the same type of reactions take place also during the formation of NW superlattices from the two other systems, rationalization becomes more complicated by the fact that π - π stacking interactions could be also operative between the phenyl groups of BA and PAA with toluene [30]. Comparing the interstitial distances obtained by the three couples, we notice that the interstitial distance is less affected by a modification of the acid than of the amine. Interestingly, the shorter and more rigid BA results to a longer interstitial distance between the NWs but thinner NW diameter, as compared to the more flexible and longer HDA. A less important increase of the interstitial distance takes place by replacing LA by PAA but in this case the NW diameter increases.

In addition to the dimensions of the nanorods and the distances that separate them from each other, the quality of the self-organization is also impacted. This is illustrated in Figure 6 with the full widths at half maximum (FWHM) of the radial (Fig. 6(a)) and azimuthal profiles of the (10) Bragg reflections (Fig. 6(b)) plotted as a function of the reaction time (Fig. 6(c)). The width of the radial profile addresses the $d_{(10)}$ -spacing dispersion, while the azimuthal profile one is related to the degree of mosaicity of the 2D hexagonal lattice. Whatever the amine/acid pair, the general trend is that both dispersion in $d_{(10)}$ -spacing and mosaicity decrease with reaction time to reach the best regular arrangement at longest reaction times. That means that, while the NW hexagonal self-organization on Pt(111) operates from the first hours of reaction, the long range order and its coherence improve up to the longest synthesis, *i.e.* 72h. Moreover, among the three amine/acid pairs that led to the regular 2D lattices of NWs, the HDA/LA is the one that results in minimal deviations from the perfect 2D hexagonal lattice as attested by the smallest FWHM in Fig. 6.

This study demonstrates that specific amine/acid pairs acting as stabilizers can lead to Co nanowires organized on Pt and presenting different characteristic lengths in terms of interwire distances and diameters. This should pave the way for a tuning of the critical distances in various nanocrystal arrays and modulations of the associated physical properties. Interestingly, the spontaneous hexagonal arrangement of the vertical nanowires on single crystalline Pt(111) is a feature that is shared by numerous, albeit not all, amine/acid pairs introduced in the reaction. Indeed, the BA/PAA pair failed to give organized nanorods. This failure provoked by the simultaneous employment of two shorter and more rigid ligands is not straightforward to explain. Steric as well as electronic properties could be responsible for the formation of Co molecular compounds that do not favor the formation of NWs. As shown in our previous works on Co nanostructures prepared in the presence of various amounts of LA and HDA in solution

[15,24], the nature and relative amount of Co species formed upon mixing the reactants dictate the resulting nano-object morphology. In this context what is surprising is not that one of the pairs does not work, but instead, the fact that taking as a reference the HDA/LA pair, replacement of either the HDA or the LA, the corresponding systems work.

For the pairs that are suitable for the self-organized growth on NWs, the SAXS analysis indicated that the final nearest-neighbor NW distance emerges up after a few hours of reaction (4h for HDA/LA) whereas the nanowires are already formed. This suggests that the long-range hexagonal order is effective in the first hours of the Co NW growth, even if the associated well-defined 6-fold symmetry SAXS pattern appears clearly from after 16h. These results indicate that the Co growth and self-organization processes are intrinsically concomitant. Then, as the reaction time increases, the degree of order of the NW superlattice improves as illustrated by the decreases of the d -spacing dispersion and of the degree of mosaicity. Organization at early reaction times, that is, as soon as elongation of the nano-objects occurs, had been also observed in the case of nanorod superlattices grown in the absence of support [24]. Nevertheless, a difference between the two processes is that while nucleation of the nanorods in the freestanding superlattices takes place in solution, where mobility of the nuclei is not restricted and allows gradual organization to be established, in the present case, the nucleation takes place on the solid support. The support being non-patterned, there is, *a priori*, no reason for nucleation to occur at regular intervals. Nevertheless, we cannot exclude a supramolecular preorganization of molecular species on the surface of the support [31-34], before the formation of the first solid entities takes place upon heating. The presence of the support could engage specific interactions with cobalt containing metallosupramolecular entities, thus fixing initial anchoring position of each NW upon nucleation. Thermal fluctuations around these initial positions during the decomposition of the molecular precursors could contribute to the improvement of the organization of the NW with time.

3. CONCLUSION

A combined monitoring by SAXS, SEM and TEM gives a comprehensive description of the concerted growth and self-organization of nanocrystals on surfaces taking place in solution. We demonstrated that apart from combining long chain amines and long chain acids as stabilizing ligands introduced in the reaction, by combining aliphatic/aromatic pairs it is also possible to grow on Pt(111) Co nanowires organized in 2D hexagonal arrays and to modulate the NW distance separation. This is an important property of the solution epitaxial growth as it illustrates the versatility of this bottom-up fabrication process. The concomitant growth and self-organization of the nanocrystals on the surfaces still need to be more deeply understood, especially the rationalization of the interparticle distance dependence on the specific amine/acid pair characteristics, as well as the possible role played by pre-organized molecular species on the substrate surface of the support prior to nanocrystal growth. The present results pave the way to the extension of this solution-based growth of nanocrystals on surfaces for the integration of different ligand-stabilized nanoparticles in planar devices.

Acknowledgements

This work was supported by the Agence Nationale de la Recherche (France) under contract No. ANR-14-CE07-0025-01 (DENSAR).

Method Section

Synthesis

All solutions were prepared in a glovebox, toluene was distilled, degassed by three freeze-pump-thaw cycles and kept in the glovebox under activated molecular sieves (Acros-Organics 4A 8-12 mesh) to remove traces of water. The metal precursor $[\text{Co}\{\text{N}(\text{SiMe}_3)_2\}_2(\text{thf})]$ was furnished by NanoMePS. Hexadecylamine (HDA) (98% Sigma Aldrich) and lauric acid (LA) (Acros) benzylamine (BA) (99.5%, Sigma Aldrich) phenylacetic acid (PAA) (99% Sigma Aldrich) were degassed and kept in the glovebox. In a representative reaction resulting in the growth of nanowires, a solution of $[\text{Co}\{\text{N}(\text{SiMe}_3)_2\}_2(\text{thf})]$ (67.8 mg, 0.15 mmol), in 1 mL of toluene is rapidly added to a mixture of HDA (72.4 mg, 0.30 mmol) and LA (60.1 mg, 0.30 mmol) in 9 mL of toluene (Co/LA/HDA molecular ratio = 1/2/2, $[\text{Co}] = 15 \text{ mM}$). The solution is introduced in a Fischer-Porter pressure bottle. The 20 nm Pt films were epitaxially grown by sputtering deposition at 500°C on 10 mm × 10 mm × 0.5 mm single crystalline $\text{Al}_2\text{O}_3(0001)$ substrate. The Pt(111)/ $\text{Al}_2\text{O}_3(0001)$ substrate was immersed in the solution with the metallic film facing the bottom of the bottle. The Fischer-Porter reactor is removed from the glovebox, the Ar is evacuated and then charged with H_2 to 3 bar. The solution containing the substrate is heated to 110°C for various reaction times between 4 and 72 h. At the end of the reaction, the solution is cooled down and the Fischer-Porter transferred to the glovebox. The substrate is removed from the solution and washed three times with toluene assisted by ultra sounds during 1 min. The same procedure is used in all experiments, with the exception of the BA/LA experiments which were performed at 130°C.

Characterization studies

Small angle neutron scattering (SAXS) measurements were performed at the Laboratoire de Genie Chimique, Toulouse, on the XEUSS 2.0 bench equipped with a copper internal source

(Genix3D) that produces an X-ray beam with an energy of 8 keV and a flow of $30 \cdot 10^6 \text{ ph. mm}^2 \cdot \text{s}^{-1}$ with a beam sized at $500 \times 500 \text{ } \mu\text{m}^2$. Each measured 2D SAXS pattern was obtained after a 4h exposure time with the X-ray beam normal to the substrate, *i.e.* parallel to the NWs. Data were collected in a transmission configuration on a $150 \times 150 \text{ mm}^2$ area DECTRIS detector (Pilatus 1M) with a sample to detector distance of 387.5 mm. The scattering intensity $I(q)$ with experimentally determined is expressed as a function of the scattering vector $q \text{ (}\text{\AA}^{-1}\text{)}$.

The FEG-SEM (field emission gun-scanning electron microscopy) observations were carried out on a JEOL JSM6700F instrument. Cross-sectional TEM lamella were prepared by Focused Ion Beam on a Thermo Fisher (FEI) Helios NanoLab 600i DualBeam. The nanowire layer was protected by a thin C layer to avoid charging effects and a thick Pt layer to avoid damages during the thinning process. The lamellae were then extracted and thinned down to about 100 nm to get electron transparency with a final step at low energy to minimize irradiation damages and amorphization of the surfaces. The cross-sectional TEM samples were investigated using a Hitachi HF2000 and a ThermoFisher Tecnai F20 fitted with a Cs corrector (CEOS) which point resolution is 0.12 nm.

Electronic Supplementary Material: Supplementary material (histograms of the nanowire diameters D determined from TEM analysis, and indexation of SAXS patterns) is available in the appendices.

Références

- [1] Boles, M. A.; Engel, M. ; Talapin, D.V. Self-Assembly of Colloidal Nanocrystals: From Intricate Structures to Functional Materials. *Chem. Rev.* **2016**, 116, 11220–11289.
- [2] Li, X.Y.; Liu, X.W.; Liu, X.G.; Self-assembly of colloidal inorganic nanocrystals: nanoscale forces, emergent properties and applications. *Chem. Soc. Rev.* **2021**, 50, 2074-2101.
- [3] Bigioni, T.P.; Lin, X.-M.; Nguyen, T.T.; Corwin, E.I.; Witten, T.A.; Jaeger, H.M. Kinetically driven self assembly of highly ordered nanoparticle monolayers. *Nat. Mat.* **2006**, 5, 265-270
- [4] Dugay, J.; Tan, R.P.; Loubat, A.; Lacroix, L.-M.; Carrey, J. Fazzini, P.F.; Blon, T.; Mayoral, A.; Chaudret, B.; Respaud, M. Tuning deposition of magnetic metallic nanoparticles from periodic pattern to thin film entrainment by dip coating method. *Lagmuir* **2014**, 30, 9028-9035
- [5] Barth, J.V.; Costantini, G.; Kern, K. Engineering atomic and molecular nanostructures at surfaces. *Nature* **2005**, 437, 671-679.
- [6] Tao, A.R.; Habas, S.; Yang, P. Shape Control of Colloidal Metal Nanocrystals. *Small* **2008**, 4, 310-325.
- [7] Bealing, C.R.; Baumgardner, W.J.; Choi, J.J.; Hanrath, T.; Hennig, R.G.; Predicting Nanocrystal Shape through Consideration of Surface-Ligand Interactions. *ACS Nano* **2012**, 6, 2118–2127
- [8] Kinge, S.; Crego-Calama, M.; Reinhoudt, D.N.; Self-Assembling Nanoparticles at Surfaces and Interfaces. *ChemPhysChem* **2008**, 9, 20–42.
- [9] Fan, H.J.; Werner, P.; Zacharias M.; Semiconductor Nanowires: From Self-Organization to Patterned Growth. *Small* **2006**, 2, 700–717
- [10] Wacaser, B.A.; Dick, K.A.; Johansson, J.; Borgström, M.T., Deppert, K.; Samuelson, L.; Preferential Interface Nucleation: An Expansion of the VLS Growth Mechanism for Nanowires. *Adv. Mater.* **2009**, 21, 153-165.

- [11] Yeo, J.; Hong, S.; Kim, G.; Lee, H.; Suh, Y.D.; Park, I.; Grigoropoulos, C.P.; Ko, S.H. Laser-Induced Hydrothermal Growth of Heterogeneous Metal-Oxide Nanowire on Flexible Substrate by Laser Absorption Layer Design. *ACS Nano* **2015**, *9*, 6059-6068.
- [12] Xu, S.; Lao, C.; Weintraub, B.; Wang, Z.L. Density-controlled growth of aligned ZnO nanowire arrays by seedless chemical approach on smooth surfaces. *J. Mater. Res.* **2008**, *23*, 2072–2077.
- [13] Srivastava, S.; Kotov, N.A.; Nanoparticle assembly for 1D and 2D ordered structures. *Soft Matter* **2009**, *5*, 1146–1156.
- [14] Wetz, F.; Soulantica, K.; Respaud, M.; Falqui, A.; Chaudret, B. Synthesis and magnetic properties of Co nanorod superlattices. *Mater. Sci. Eng. C* **2007**, *27*, 1162–1166.
- [15] Liakakos, N.; Cormary, B.; Li, X.; Lecante, P.; Respaud, M.; Maron, L.; Falqui, A.; Genovese, A.; Vendier, L.; Koïnis, S.; *et al.* The Big Impact of a Small Detail: Cobalt Nanocrystal Polymorphism as a Result of Precursor Addition Rate during Stock Solution Preparation. *J. Am. Chem. Soc.* **2012**, *134*, 17922–17931.
- [16] Liakakos, N.; Blon, T.; Achkar, C.; Vilar, V.; Cormary, B.; Tan, R.P.; Benamara, O.; Chaboussant, G.; Ott, F.; Warot-Fonrose, B.; *et al.* Solution Epitaxial Growth of Cobalt Nanowires on Crystalline Substrates for Data Storage Densities Beyond 1Tbit/in². *Nano Lett.* **2014**, *14*, 3481–3486.
- [17] Harmel, J.; Peres, L.; Estrader, M.; Berliet, A.; Maury, S.; Fécant, A.; Chaudret, B.; Serp, P.; Soulantica, K. hcp-Co nanowires grown on metallic foams as catalysts for the Fischer-Tropsch synthesis. *Angew. Chem. Int. Ed.*, **2018**, *57*, 10579–10583.
- [18] Lacroix, L.-M. ; Lachaize, S. ; Falqui, A.; Respaud, M.; Chaudret, B. Iron Nanoparticle Growth in Organic Superstructures. *J. Am. Chem. Soc.* **2009**, *131*, 549–557.

- [19] Peres, L.; Yi, D.; Bustos-Rodriguez, S.; Garcia-Marcelot, C.; Pierrot, A.; Fazzini, P.F.; Florea, I.; Arenal, R.; Lacroix, L.M.; Warot-Fonrose, B.; *et al.* Shape-selection through epitaxy of supported platinum nanocrystals. *Nanoscale* **2018**, 10, 22730-22736.
- [20] Liakakos, N.; Achkar, C.; Cormary, B.; Harmel, J.; Warot-Fonrose, B.; Snoeck, E.; Chaudret, B.; Respaud, M.; Soulantica, K.; Blon, T.; Oriented Metallic Nano-Objects on Crystalline Surfaces by Solution Epitaxial Growth. *ACS Nano* **2015**, 9, 9665-9677.
- [21] Albrecht, T.R.; Arora, H.; Ayanoor-Vitikate, V.; Beaujour, J-M.; Bedau, D.; Berman, D.; Bogdanov, A.L.; Chapuis, Y-A.; Cushen, J.; Dobisz, E.E.; *et al.* Bit-Patterned Magnetic Recording: Theory, Media Fabrication, and Recording Performance. *IEEE Trans. Magn.* **2015**, 51, 0800342.
- [22] Sun, S. H.; Murray, C. B.; Weller, D.; Folks, L.; Moser, A.; Monodisperse FePt nanoparticles and ferromagnetic FePt nanocrystal superlattices. *Science* **2000**, 287, 1989–1992
- [23] Li, T.; Senesi, A.J.; Lee, B. Small Angle X-ray Scattering for Nanoparticle Research. *Chem. Rev.* **2016**, 116, 11128–11180
- [24] Cormary, B.; Li, T.; Liakakos, N.; Peres, L.; Fazzini, P-F.; Blon, T.; Respaud, M.; Kropf, A.J.; Chaudret, B.; Miller, J.T.; *et al.* Concerted growth and ordering of cobalt nanorod arrays as revealed by tandem in situ SAXS-XAS studies. *J. Am. Chem. Soc.* **2016**, 138, 8422–8431.
- [25] Dumestre, F.; Chaudret, B.; Amiens, C.; Respaud, M.; Fejes, P.; Renaud, P.; Zurcher, P. Unprecedented Crystalline Super-Lattices of Monodisperse Cobalt Nanorods. *Angew. Chem. Int. Ed.* **2003**, 42, 5213 –5216.
- [26] Whetten, R.L.; Shafigullin, M.N.; Khoury, J.T.; Schaaff, T.G.; Vezmar, I.; Alvarez, M.M.; Wilkinson, A. Crystal Structures of Molecular Gold Nanocrystal Arrays. *Acc. Chem. Res.* **1999**, 32, 397-406.

- [27] Boles, M.A.; Talapin, D.V. Many-Body Effects in Nanocrystal Superlattices: Departure from Sphere Packing Explains Stability of Binary Phases. *J. Am. Chem. Soc.* **2015**, *137*, 4494–4502.
- [28] Quan, Z.; Xu, H.; Wang, C.; Wen, X.; Wang, Y.; Zhu, J.; Li, R.; Sheehan, C.J.; Wang, Z.; Smilgies, D.M.; *et al.* Solvent-Mediated Self-Assembly of Nanocube Superlattices. *J. Am. Chem. Soc.* **2014**, *136*, 1352–1359.
- [29] Kazmierczak, K.; Yi, D.; Jaud, A.; Fazzini, P.F.; Estrader, M.; Viau, G.; Decorse, P.; Piquemal, J.Y.; Michel, C.; Besson, M.; *et al.* Influence of Capping Ligands on the Catalytic Performances of Cobalt Nanoparticles Prepared with the Organometallic Route. *J. Phys. Chem. C* **2021**, *125*, 7711–7720.
- [30] Feng, X.; Sosa-Vargas, L.; Umadevi, S.; Mori, T.; Shimizu, Y.; Hegmann, T. Discotic Liquid Crystal-Functionalized Gold Nanorods: 2- and 3D Self-Assembly and Macroscopic Alignment as well as Increased Charge Carrier Mobility in Hexagonal Columnar Liquid Crystal Hosts Affected by Molecular Packing and π – π Interactions. *Adv. Funct. Mater.* **2015**, *25*, 1180–1192.
- [31] Lin N.; Stepanow S.; Ruben M.; Barth J.V. Surface-Confined Supramolecular Coordination Chemistry. In: Broekmann P., Dötz KH., Schalley C.A. (eds) *Templates in Chemistry III. Topics in Current Chemistry* **2008**, 287 Springer, Berlin, Heidelberg.
- [32] Lippel, P.H.; Wilson, R.J.; Miller, M.D.; Wöll, C.; Chiang, S. High-Resolution Imaging of Copper-Phthalocyanine by Scanning-Tunneling Microscopy. *Phys. Rev. Lett.* **1989**, *62*, 171–174.
- [33] Kröger, J.; Jensen, H.; Néel, N.; Berndt, R. Self-organization of cobalt-phthalocyanine on a vicinal gold surface revealed by scanning tunnelling microscopy. *Surf. Sci.* **2007**, *60*, 4180–4184.

[34] Barth, J.V.; Molecular Architectonic on Metal Surfaces. *Annu. Rev. Phys. Chem.* **2007**, *58*, 375–407.

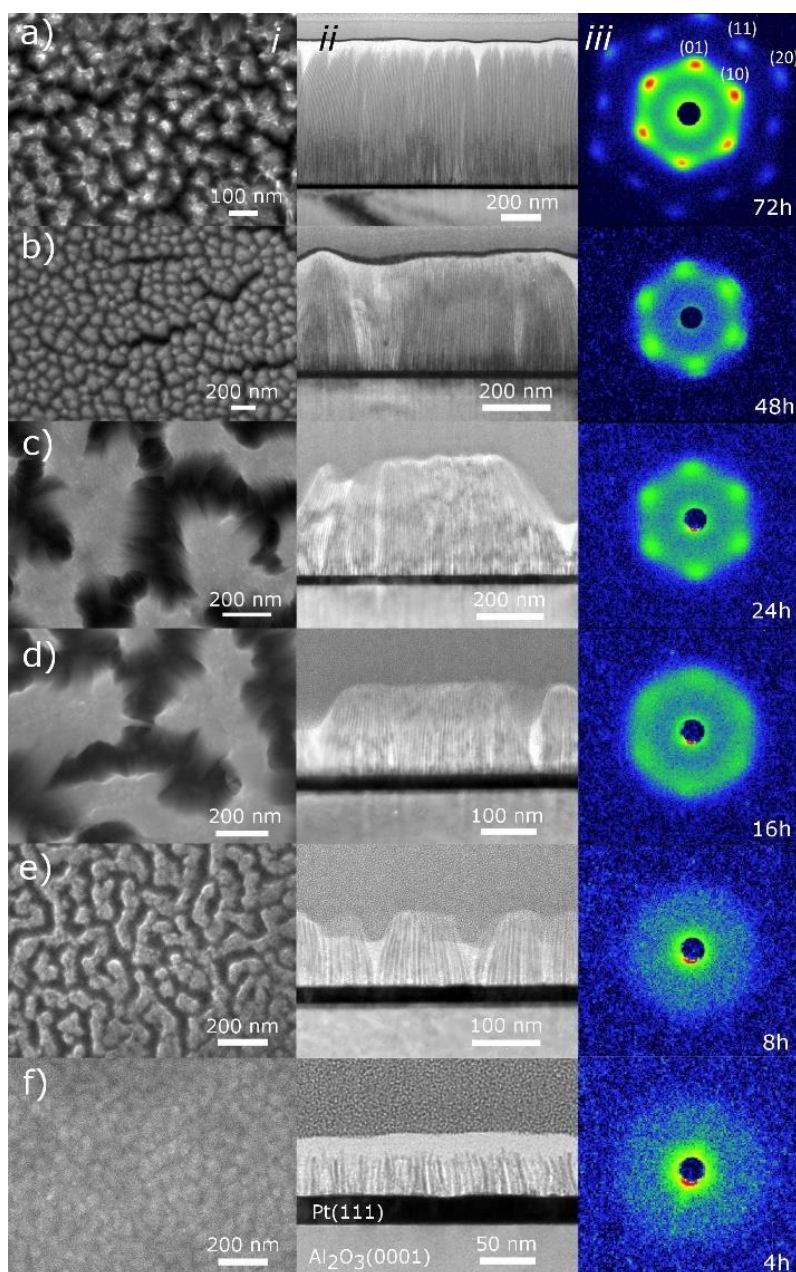


Figure 1: (i) SEM, (ii) TEM micrographs, and (iii) SAXS patterns (transmission mode, normal to the substrate) obtained after synthesis with Co/HDA/LA for different reaction times : a) 72h, b) 48h, c) 24h, d) 16h, e) 8h and f) 4h. (10), (20) and (11) in (iii) refer to the (*hk*) Bragg indices of the 2D hexagonal lattice of Co NWs (Co/HDA/LA ratio: 1/2/2, [Co] = 15 mM, 110 °C, solvent: toluene).

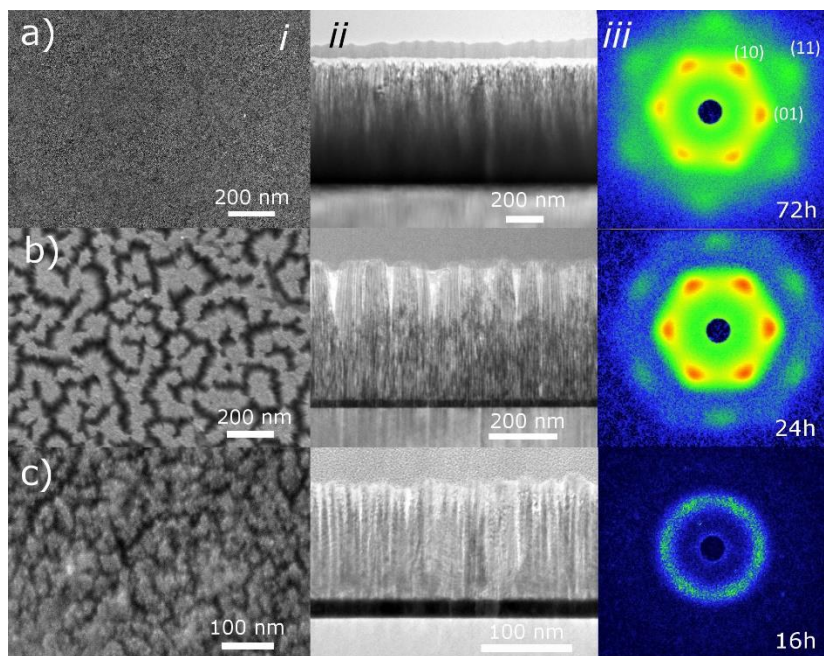


Figure 2: (i) SEM, (ii) TEM micrographs and (iii) SAXS patterns (transmission mode, normal to the substrate) obtained after synthesis with Co/HDA/PAA for different reaction times: a) 72h, b) 24h, d) 16h (Co/HDA/PAA ratio: 1/2/2, [Co] = 15 mM, 110 °C, solvent: toluene).

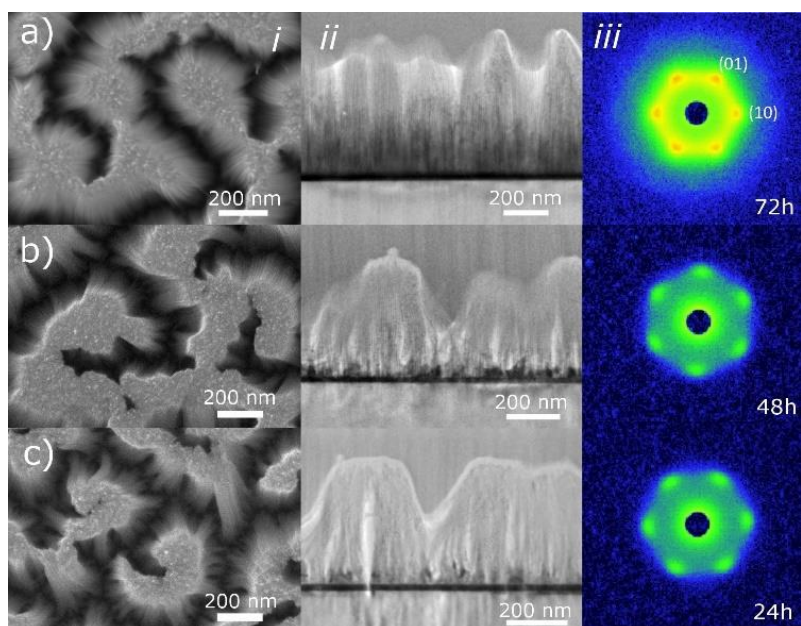


Figure 3: (i) SEM, (ii) TEM micrographs and (iii) SAXS patterns (transmission mode, normal to the substrate) obtained after synthesis with Co/BA/LA for different reaction times: a) 72h, b) 48h, c) 24h, (Co/BA/LA ratio: 1/2/2, [Co] = 15 mM, 130 °C, solvent: toluene).

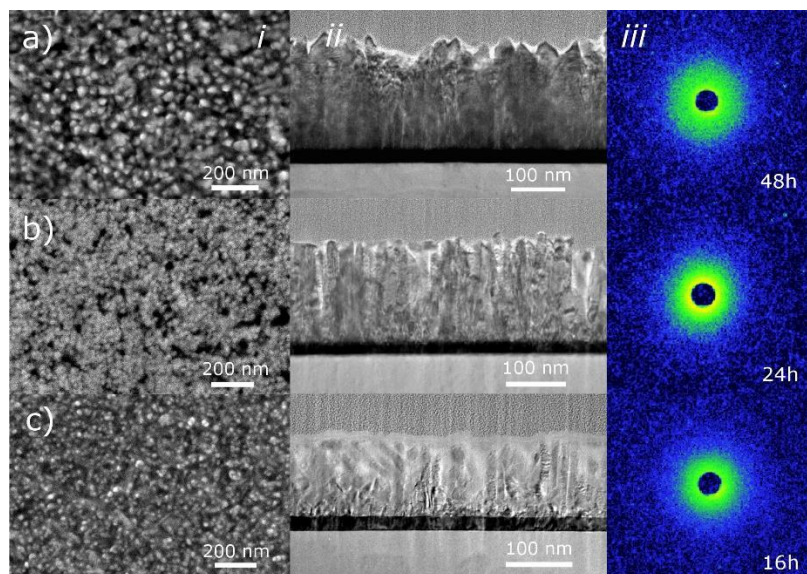


Figure 4: (i) SEM, (ii) TEM micrographs and (iii) SAXS patterns (transmission mode, normal to the substrate) obtained after synthesis with Co/BA/PAA for different reaction times: a) 48h, c) 24h, d) 16h (Co/BA/PAA ratio: 1/2/2, [Co] = 15 mM, 110 °C, solvent: toluene).

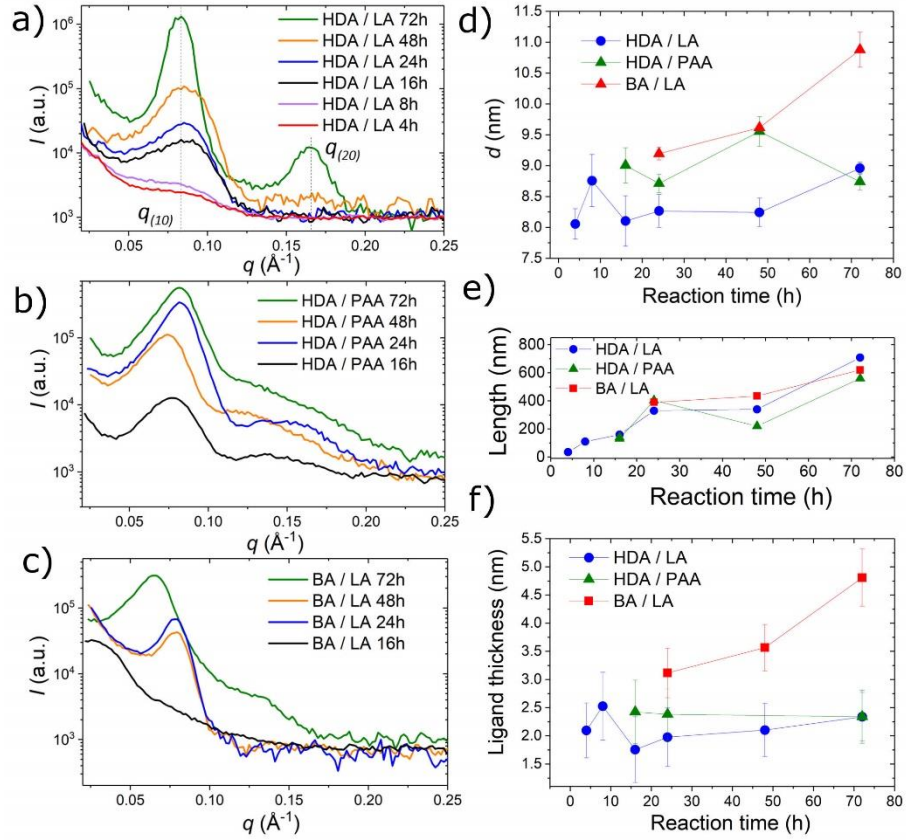


Figure 5 : Radial scattering intensity profiles $I(q)$ determined from the SAXS patterns of a) HDA / LA (Fig. 1(iii)), (b) Fig. 2(iii) HDA / PAA (Fig. 2(iii)), and c) BA / LA (Fig. 3(iii)). d) Inter-reticular spacing d deduced from the first peak position $q_{(10)}$ in SAXS patterns ($d = 2\pi/q_{(10)}$). e) NW length measured on TEM micrographs as a function of reaction time. f) ligand shell thickness as a function of the reaction time.

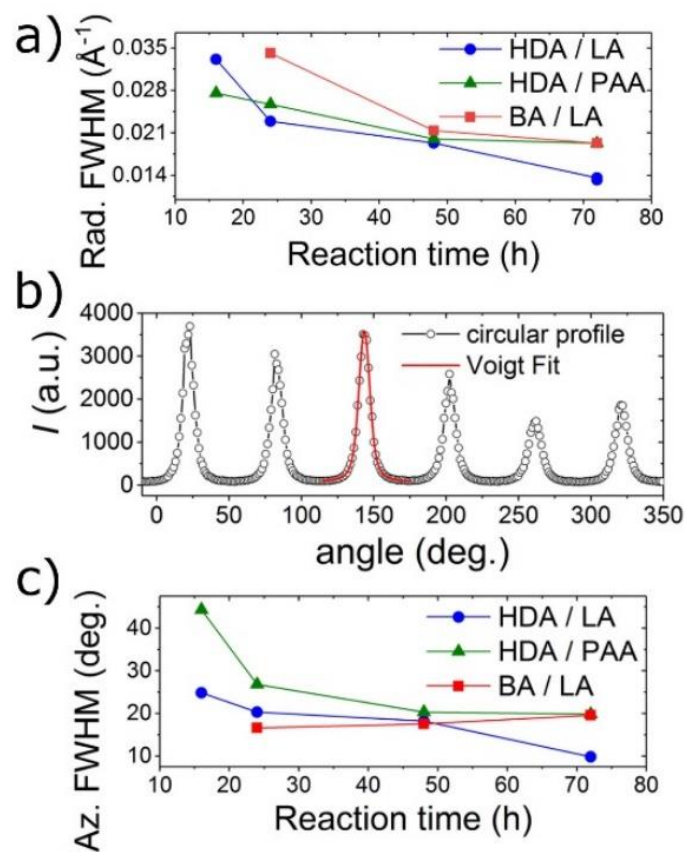


Figure 6: (a) Full width at half maximum (FWHM) of the (10) SAXS peak determined from the radial profile $I(q)$ plotted in Fig. 2(a),(b),(c) for HDA/LA, HDA/PAA and BA/LA respectively, and plotted as function of the reaction time. (b) Azimuthal profile of the (10) reflections for HDA/LA (72h) SAXS pattern (Fig. 1(a)(iii)) and associated Voigt fit. (c) FWHM of the azimuthal profiles of the (10) reflections for the different amine/acid pairs as a function of the reaction time.

Electronic Supplementary Information for
Self-organization and tunable characteristic lengths of two-dimensional hexagonal
superlattices of nanowires directly grown on substrates

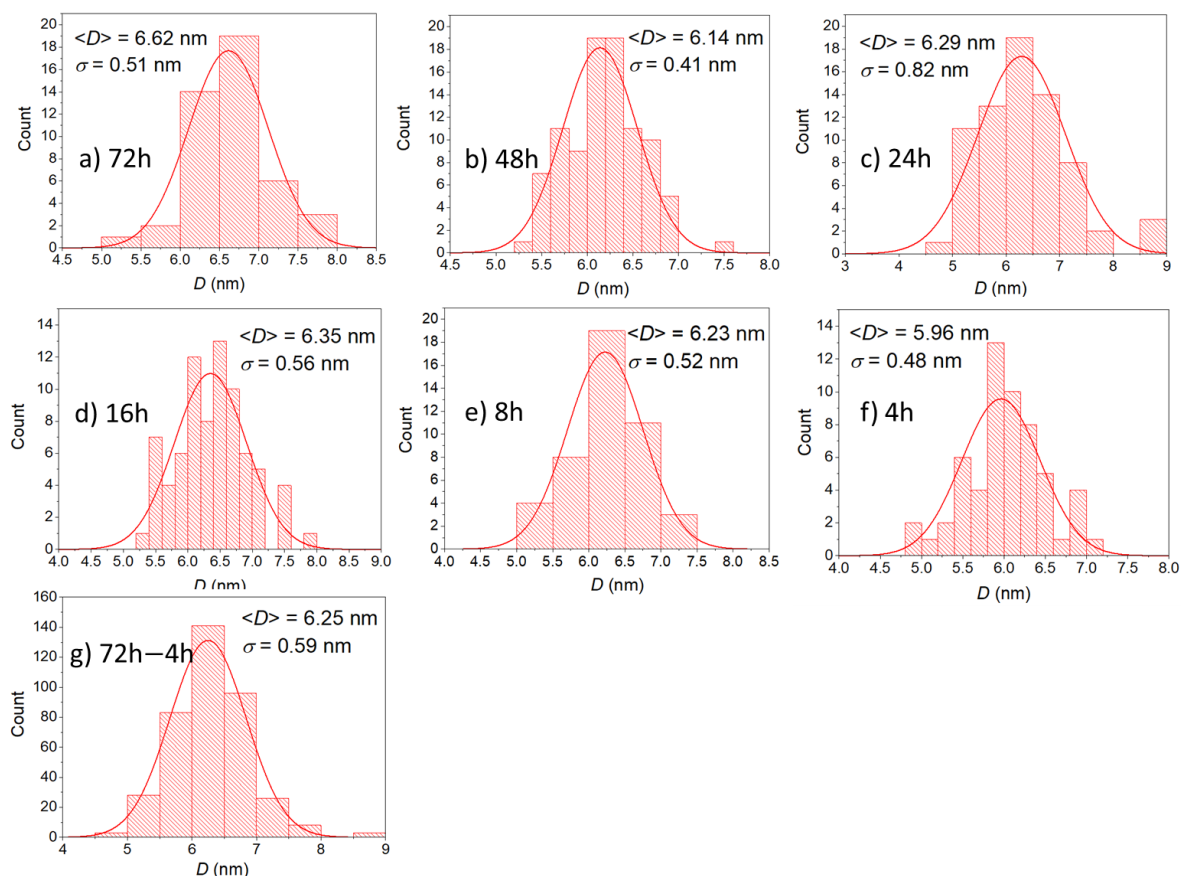


Figure S1 : Histograms of the nanowire diameters D determined from the cross-sectional TEM micrographs and their associated fits with normal functions. From TEM analysis performed after synthesis with Co/HDA/LA for different reaction times : a) 72h, b) 48h, c) 24h, d) 16h, e) 8h and f) 4h. g) Histogram of the nanowire diameters D for the entire 72h-4h time range and the associated fit.

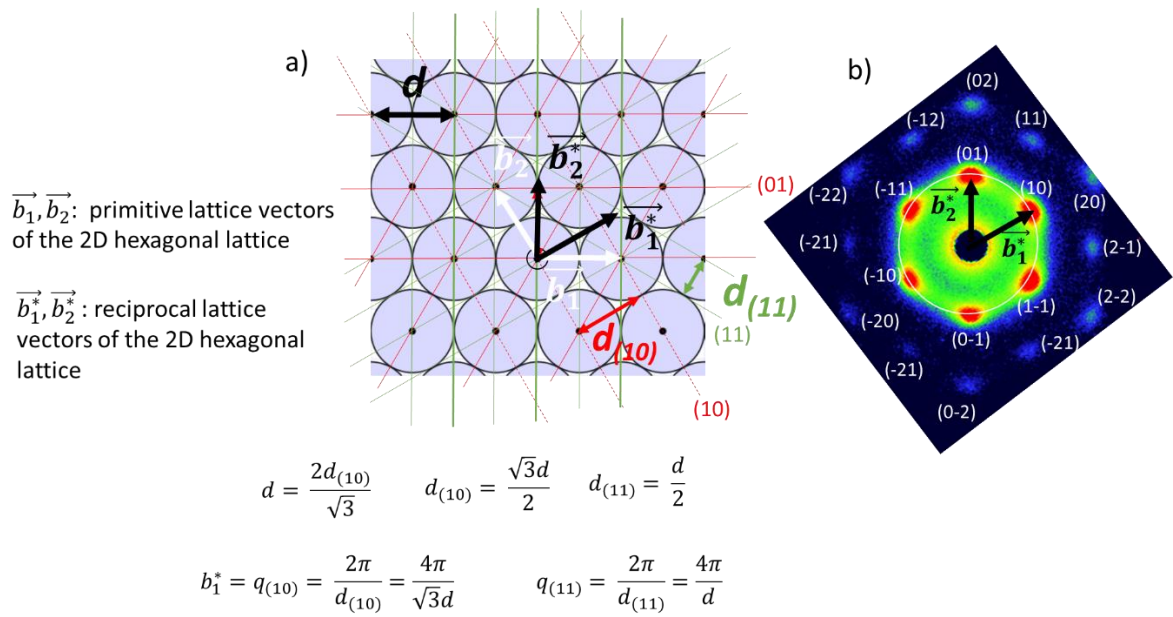


Fig. S2: a) direct 2D hexagonal lattice of vertical nanowires with corresponding vectors \vec{b}_1, \vec{b}_2 , reciprocal vectors \vec{b}_1^*, \vec{b}_2^* and interplanar distances. b) indexation of a SAXS pattern with the (hk) Bragg indices corresponding to the 2D hexagonal lattice of Co NWs.

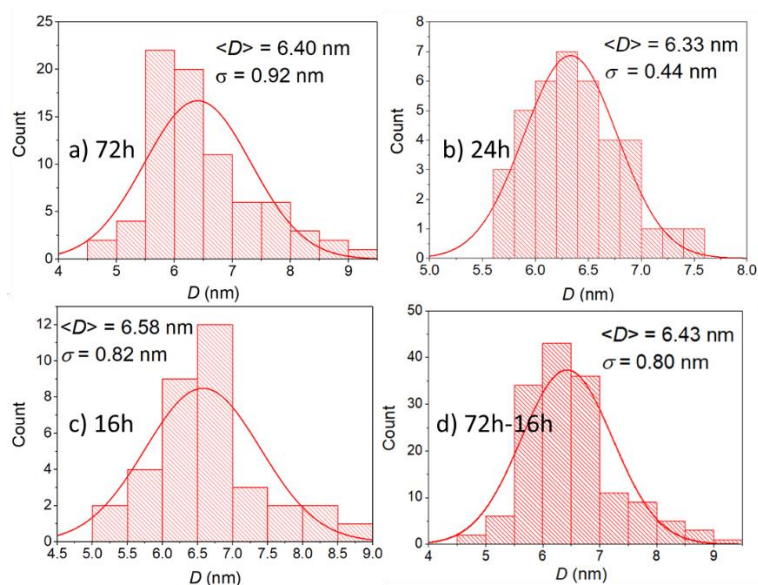


Figure S3 : Histograms of the nanowire diameters D determined from the cross-sectional TEM micrographs and their associated fits with normal functions. From TEM analysis performed after synthesis with Co/HDA/PAA for different reaction times : a) 72h, b) 24h, c) 16h. d) Histogram of the nanowire diameters D for the entire 72h-16h time range and the associated fit.

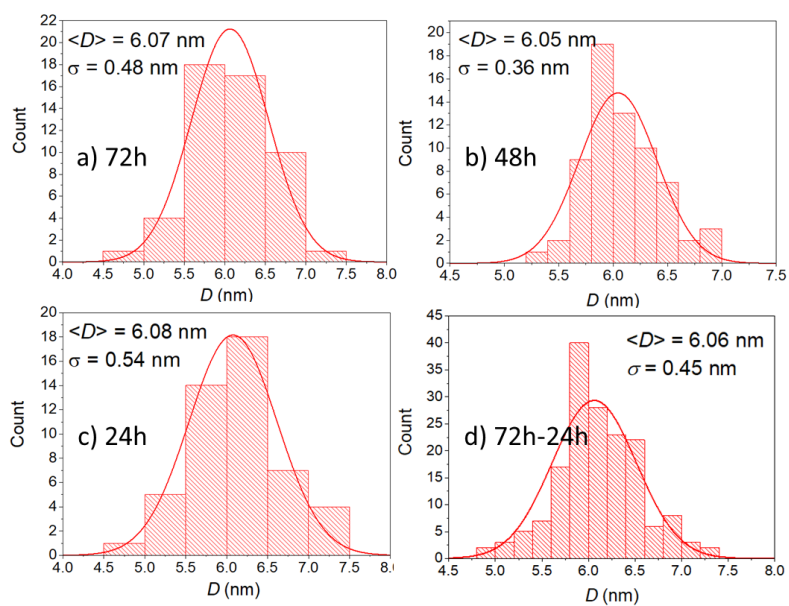


Figure S4 : Histograms of the nanowire diameters D determined from the cross-sectional TEM micrographs and their associated fits with normal functions. From TEM analysis performed after synthesis with Co/BA/LA for different reaction times : a) 72h, b) 48h, c) 24h. d) Histogram of the nanowire diameters D for the entire 72h-24h time range and the associated fit.